CJC Chinese Journal of Chemistry 中国化学 - An International Journal

For submission: https://mc.manuscriptcentral.com/cjoc
For published articles: https://onlinelibrary.wiley.com/journal/16147065

Concise Report

Cite this paper: *Chin. J. Chem.* **2024**, *42*, 1456—1464. **DOI: 10.1002/cjoc.202300723**

A DNA Force Circuit for Exploring Protein-Protein Interactions at the Single-Molecule Level†

Kangkang Ma,[a] Luoan Xiong,[b] Zhuofei Wang,[a] Xin Hu,[a] Lihua Qu,[a] Xuetong Zhao,[a] Yao Li,*[,b] and Zhongbo Yu*[,a]

[a] *State Key Laboratory of Medicinal Chemical Biology, Frontiers Science Center for Cell Responses, and College of Pharmacy, Nankai University, 38 Tongyan Road, Tianjin 300350, China*
[b] *School of Physics and Key Laboratory of Functional Polymer Materials of Ministry of Education, Nankai University, and Collaborative Innovation Center of Chemical Science and Engineering, Tianjin 300071, China*

Keywords

Single-molecule studies | Protein-protein interactions | Click chemistry | Genetic code expansion | Molecular dynamics

Comprehensive Summary

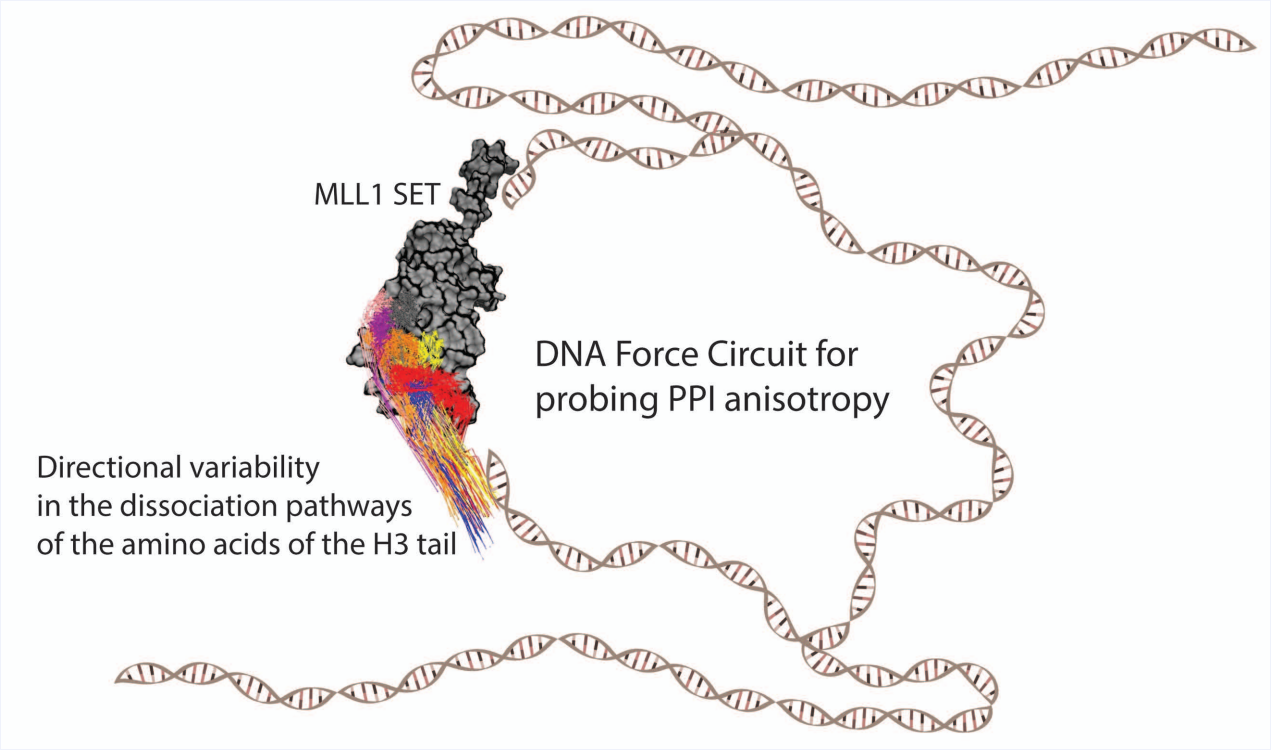

Protein-protein interactions (PPIs) play a crucial role in drug discovery and disease treatment. However, the development of effective drugs targeting PPIs remains challenging due to limited methodologies for probing their spatiotemporal anisotropy. Here, we propose a single-molecule approach using a unique force circuit to investigate PPI dynamics and anisotropy under mechanical forces. Unlike conventional techniques, this approach enables the manipulation and real-time monitoring of individual proteins at specific amino acids with defined geometry, offering insights into molecular mechanisms at the single-molecule level. The DNA force circuit was constructed using click chemistry conjugation methods and genetic code expansion techniques, facilitating orthogonal conjugation between proteins and nucleic acids. The SET domain of the MLL1 protein and the tail of histone H3 were used as a model system to demonstrate the application of the DNA force circuit. With the use of atomic force microscopy and magnetic tweezers, optimized assembly procedures were developed. The DNA force circuit provides an exceptional platform for studying the anisotropy of PPIs and holds promise for advancing drug discovery research targeted at PPIs.

*E-mail: zyu@nankai.edu.cn; liyao@nankai.edu.cn
† Dedicated to the Special Issue of Single-Molecule Measurement and Imaging.

Background and Originality Content

Protein-protein interactions (PPIs) hold promise as targets for drug discovery, presenting significant opportunities for therapeutic modulation in disease treatment.[1] PPIs can occur as homomeric or heteromeric interactions, exhibiting diverse strengths and durations. According to PPI databases, the binding affinity for PPIs crosses six orders of magnitude, ranging from picomolar to micromolar.[2] Obligate PPIs are characterized by strong and long-lived interactions, while non-obligate interactions are typically weaker and more transient.

The significant role of direct PPIs in diseases has received widespread recognition. However, the availability of drugs that effectively disrupt PPIs remains limited, highlighting the challenges in transforming them into viable targets for drug discovery. PPIs involve both the globular protein and the peptide chain at their interface. Understanding the secondary structural features, such as α-helices and β-strands, within the peptide chain is crucial for designing inhibitors that can mimic and displace these peptides.[3] The energetics and kinetics of the interactions are essential for comprehending the underlying principles of PPIs.[4]

Structural studies of PPIs are commonly supported by X-ray crystallography and nuclear magnetic resonance (NMR) spectroscopy. Bioinformatic approaches also contribute to the detection of PPIs. Additionally, there are other techniques for investigating PPIs, such as surface plasmon resonance, microscale thermophoresis, and electrophoretic mobility shift assay, among others. However, these techniques have their limitations as they do not consider the spatiotemporal anisotropy of PPIs. They typically evaluate the strength of PPIs based on bulk concentration, which may not accurately reflect the anisotropy of structures, making it less reliable for drug discovery.[5] Previous research has shown the presence of mechanical anisotropy in protein stabilities, both at the structural and single-molecule level.[6] PPI anisotropy may be influenced by mechanostability, which is determined by hydrogen bonds and interactions facilitated by membrane elastic deformations. Conventional techniques do not provide insights into PPI anisotropy subjected to the mechanical forces encountered in cellular environments.[7]

Unlike conventional methods mentioned earlier, single-molecule mechanical techniques, such as atomic force microscopy (AFM), optical tweezers, or magnetic tweezers, are powerful tools for elucidating the mechanical details of PPIs under forces, offering a unique approach in drug discovery research.[8] These techniques enable the manipulation of individual molecules, particularly large biological macromolecules, and real-time monitoring of their spatiotemporal responses under mechanical loads. They offer insights into complex molecular events such as drug targeting, molecular interactions, and conformational changes, enabling the dynamic analysis of molecular mechanisms at the single-molecule level.[9]

Typically, single-molecule manipulation strategies involve the placement of affinity tags at both ends of the biological macromolecule, for example, at the 3' and 5' ends of nucleic acids or the N and C termini of proteins.[7a,10] These tags allow for the application of forces on both ends of the molecule via affinity interactions, allowing the investigation of single-molecule dynamics of nucleic acids, proteins, and their target drugs.[9b,11] However, these single-molecule mechanical strategies use only one manipulation geometry, which corresponds to the backbone of the biological macromolecule, such as the phosphate backbone of nucleic acids or the peptide bond backbone of proteins. Due to the limitation of manipulation geometry, single-molecule techniques are particularly suitable for manipulating one molecule. To investigate interactions between two molecules, a common strategy is to manipulate one molecule while allowing the other molecule to freely diffuse in the reaction solution. To simultaneously manipulate two molecules, the current strategy makes the two molecules in a serial arrangement, such as engineering two interacting proteins into a fusion protein with a flexible linker as an isolating sequence.[12] However, this fusion protein strategy, which applies forces to the beginning and ending amino acids, cannot mechanically probe the PPI anisotropy at any desired amino acid positions. Recently, our lab, along with others, has developed a strategy that employs a DNA force circuit for detecting PPIs, directly revealing the interaction forces and residence times for PPI-targeted drug discovery.[13] Furthermore, the force circuit strategy incorporates the genetic code expansion method,[14] enabling us to select virtually any amino acids for mechanical manipulations. This breakthrough allows us to study PPI anisotropy with precise control over the molecular geometry.

In this study, we provide a detailed demonstration of the DNA force circuit. One path is dedicated to detecting protein interactions, while the other maintains the single-molecule experimental architecture. We used this DNA force circuit to investigate the interactions between the SET domain of MLL1 protein and the tail of histone H3. To construct the DNA force circuit, we employed click chemistry conjugation methods to create DNA branching points and genetic code expansion techniques to insert highly reactive unnatural amino acids into the protein. This approach enabled the orthogonal conjugation between proteins and nucleic acids, assisting the construction of the DNA force circuit. With the use of atomic force microscopy, we optimized the preparation and assembly procedures of the single-molecule DNA force circuit. The DNA force circuit serves as a unique single-molecule platform for studying PPI anisotropy.

Results and Discussion

PPI anisotropy in MLL1 SET-H3 complex revealed by MD simulation

In this study, we used molecular dynamics (MD) simulations to investigate the spatiotemporal anisotropy in protein-protein interactions (PPIs) between MLL1 SET and the tail of histone 3 (Figure 1). The initial coordinates of the MLL1 SET-H3 complex for the MD simulation were obtained from the Protein Data Bank (PDB) entry 2W5Z and set up using GROMACS software (Figure 1A).[15] The MD system consisted of 160 000 atoms and was set at pH 7.4 with 100 mmol·L^{-1} NaCl, along with water molecules. Prior to the pulling process, the system's energy was minimized until the force dropped below 1000 (kJ/mol)/nm. To initiate the pulling process, harmonic restraints with a spring constant of 500 (kJ/mol)/nm^2 were applied to the α-C atoms of H3 peptide. Specifically, the α-C atoms of residues 2-THR, 4-GLN, 5-THR, and 8-TYR were chosen as the force pulling points, and a constant force of 200 (kJ/mol)/nm was exerted on these atoms (Figure 1B). The pulling simulation was conducted with a time step of 2 fs.

Our findings indicate that the dissociation time of the H3 peptide from the MLL1 SET binding pocket is significantly influenced by the direction of the applied forces and the pulling sites on the substrate peptide. As a result, dissociation times of 5.33 ns, 2.20 ns, 3.30 ns, and 3.27 ns were observed for residues 2-THR, 4-GLN, 5-THR, and 8-TYR, respectively. Additionally, upon applying the pulling forces, the centers of mass of the eight amino acids exhibited distinct detaching trajectories and showed significant structural changes in the complex (Figures 1C—F). Snapshots during the process of pulling the α-C atom of residue 4-GLN in H3 demonstrate a typical detaching trajectory (Figure S1). Our MD results provide insights into the anisotropy (directional dependence) of the PPI dissociation process and reveal the specific response of amino acids to external forces during the pulling simulation.

Our previous work has shown that single-molecule manipulation tools are unique in investigating PPI anisotropy. Specifically, we have developed a DNA force circuit strategy that utilizes the genetic code expansion method to selectively choose amino acids

for precise mechanical manipulations based on desired molecular geometry. It is crucial to optimize the preparation process of the DNA force circuit, which will allow for more efficient and accurate investigation of PPI anisotropy.

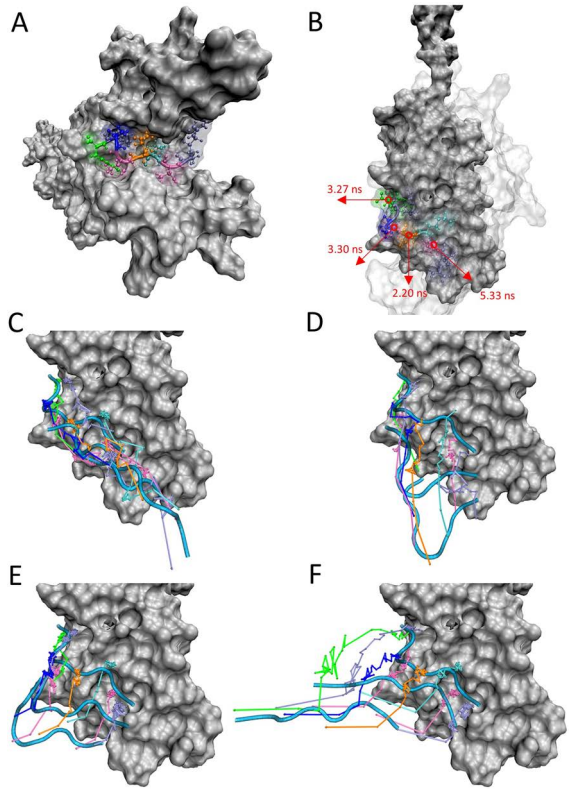

Figure 1 Anisotropy of PPI dissociation revealed by molecular dynamics pulling simulation. (A) Initial structure of the MLL1 SET-Histone 3 complex for the pulling process, illustrating the H3 substrate peptide from the N-terminus (right) to the C-terminus (left), arranged as follows: ARG (ice blue) - THR (mauve) - LYS (cyan) - GLN (orange) - THR (mauve) - ALA (blue) - ARG (ice blue) - TYR (green). The side view of the complex is derived from PDB entry 2W5Z. (B) Top view of the initial structure of the pulling process, illustrating the directions of applied forces (indicated by arrows), the pulling sites at the amino acids of H3 (α-C atom of residues 2-THR, 4-GLN, 5-THR, and 8-TYR), and the average dissociation times in four different directions. (C—F) Upon applying a force of 200 (kJ/mol)/nm to the α-C atom of residues 2-THR (C), 4-GLN (D), 5-THR (E), and 8-TYR (F), the trajectories of the centers of mass of the eight amino acids are depicted (Every ten frames, take a point, and then connect each point in sequence.), along with the structural evolution of the H3 peptide at three different time points (partial data).

Branched DNA handles used in the DNA force circuit for single-molecule PPI assays

The construction of branched DNA handles used in the single-molecule DNA force circuit consists of affinity modification components and branching components. Affinity modifications come from the digoxigenin- and biotin-modified PCR primers (Figure 2A). The branching components in the DNA for DNA force circuit require bioconjugate chemistry of which we employed copper-catalyzed azide-alkyne cycloaddition (CuAAC) to create branching points. Alkyne and azide oligos were used to generate branched primers, which were then utilized to prepare affinity handles with branching points. The affinity handles were further connected to conventional PCR-prepared linker, DNA handle L. In the DNA force circuit, we also used CuAAC to synthesize the H and S branch primers, where H stands for histone and S for SET. The digoxigenin handle carries the H branching point for anchoring the tail of histone 3, while the biotin handle carries the S branching point for anchoring the SET domain of MLL1 protein.

Considering the kinetic theory of local equilibrium, the reaction rate of this click chemistry reaction is influenced by various factors, such as the source of copper ions, ligand, reducing agent, temperature, substrate molar ratio, shaking, and ambient gas.[16] Previously, we have tested reaction conditions such as the source of copper ions, ligand, and reducing agent.[13a] We specifically investigated the substrate molar ratio, shaking, ambient gas, temperature, and reaction time (Figures 2B—C). The optimized reaction conditions consist of a substrate molar ratio of 2 : 1, a temperature of 30 °C, nitrogen gas purged, and shaking at 40 r/min for 4 h (Figure 2B, lane 9; Figure 2C, lane 7), as revealed by gel quantification (Figure S2). The reaction efficiency currently allows for the almost complete consumption of one of the two substrates.

We next purified the three DNA fragments, DNA handle L, biotin handle with the S branching point, and digoxigenin handle with the H branching point (Figure 2D). The final ligation efficiency of DNA handles, calculated based on the substrate, is approximately 20%—30% (Figure 2E). The molecular morphology of the final DNA handle was characterized using atomic force microscopy (AFM). The nucleic acid molecules exhibited equal lengths (647 ± 55 nm, n = 48), consistent with the theoretically expected lengths (Figure 2F and Figure S3).

Bioconjugation between the SET domain of MLL1 protein and DNA

We expressed and purified the MLL1 SET protein in *E. coli*. Subsequently, we used the genetic code expansion technique to introduce an unnatural amino acid, 4-azido-*L*-phenylalanine (AzF), at the N-terminus of the MLL1 SET protein for protein-DNA conjugation.[17] The gene sequence of the target protein MLL1 SET was inserted into the pET-28a vector, regulated by a lactose-controlled operator, and required IPTG activation for expression, with the unnatural amino acid encoded by the amber codon UAG. Previously, our lab used the plasmid pEVOL-AzF to express the tRNA and aminoacyl-tRNA synthetase (aaRS) required for the genetic code expansion.[13a,18] The plasmid pEVOL-AzF contains an arabinose-controlled operator, enabling efficient expression of the tRNA and aaRS to translate the amber codon into the unnatural amino acid.[19] However, there has been a problem of low expression efficiency using the plasmid pEVOL-AzF. To improve the expression level, glycerol and DMSO were supplemented in the culture medium.[13a] The typical expression conditions previously used were LB medium, cultivation temperature of 37 °C, induction temperature of 25 °C, IPTG of 0.2 mmol/L, arabinose of 0.2%, supplemented with 10 μmol/L $ZnCl_2$, and addition of 5% glycerol or 5% DMSO. In order to further investigate the effects of glycerol and DMSO on bacterial expression, we here optimized the conditions and found that under conditions where only zinc ions were supplemented, the protein was not expressed, and the various combinations of glycerol and DMSO in the culture medium did not significantly improve the expression level of the protein (Figure S4A).

We also expressed the tRNA and aaRS using another plasmid, pEVOLCNF-RS.[20] After co-transformation of pEVOLCNF-RS and the MLL1 AzF-SET plasmid, we cultured bacteria in 2xYT medium supplemented with 20 μg/mL chloramphenicol and 25 μg/mL kanamycin. To investigate the effect of the operator in the protein expression conditions, we also increased the arabinose dose from 0.02% to 0.2% and decreased the IPTG dose from 1 mmol/L to 0.2 mmol/L. Nevertheless, we found that neither glycerol nor DMSO is necessary for the expression of the MLL1 AzF-SET using the plasmid pEVOLCNF-RS (Figure S4B).

We further carefully examined the conditions for the expression of MLL1 AzF-SET using the plasmid pEVOLCNF-RS. Under the condition without any additives at 25 °C, MLL1 AzF-SET was not expressed (Figure S5A, lane 1). With the addition of IPTG and

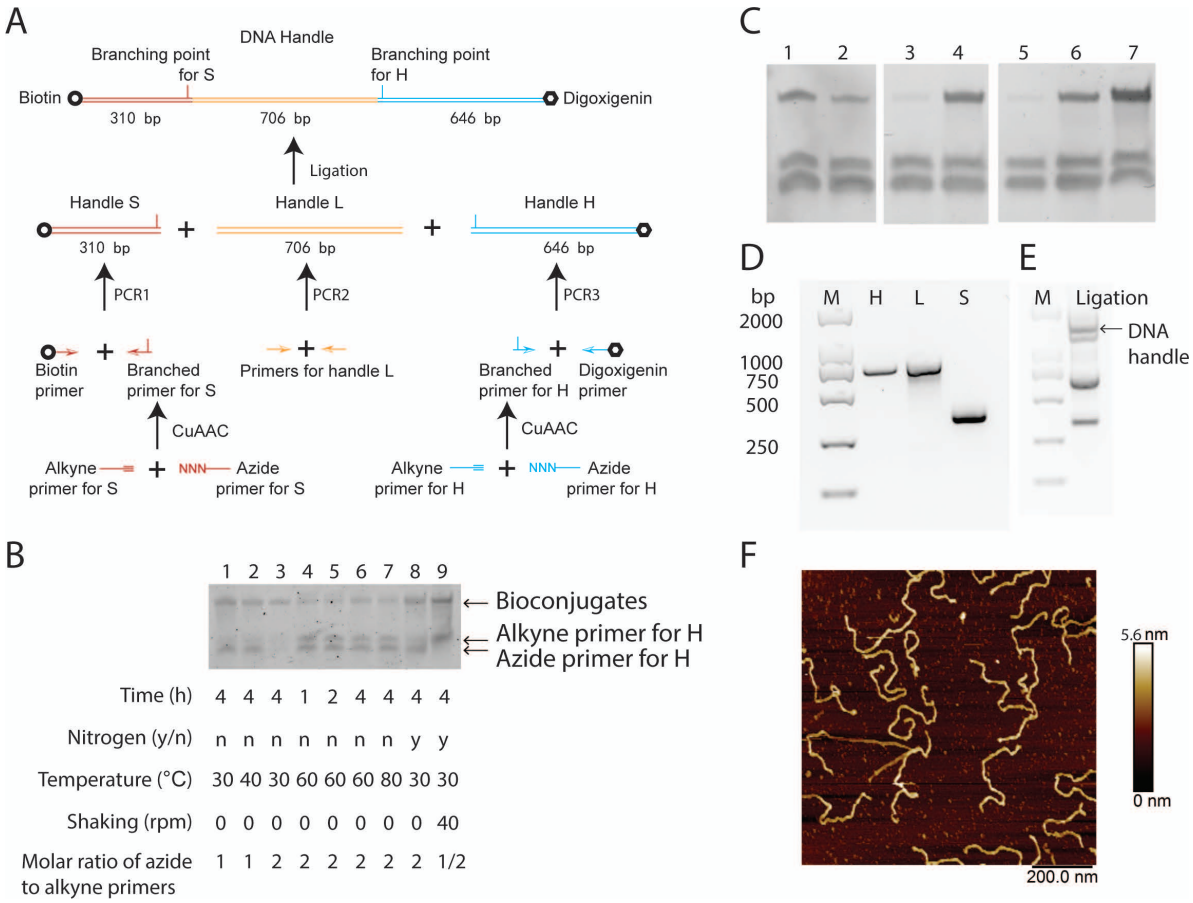

Figure 2 Optimization of the preparation procedure of branched DNA handles. (A) Flowchart illustrating the preparation procedure of branched DNA handles. (B) Optimization of CuAAC conditions for branched primer H. (C) Optimization of CuAAC conditions for branched primer S. Reaction conditions are as follows: Lane 1: 4 h reaction without shaking, molar ratio of azide to alkyne primers = 1, 30 °C, not nitrogen purged. Lane 2: 4 h reaction without shaking, molar ratio of azide to alkyne primers = 1, 40 °C, not nitrogen purged. Lane 3: 1 h reaction without shaking, molar ratio of azide to alkyne primers = 2, 37 °C, not nitrogen purged. Lane 4: 1 h reaction without shaking, molar ratio of azide to alkyne primers = 2, 37 °C, nitrogen purged. Lane 5: 4 h reaction without shaking, molar ratio of azide to alkyne primers = 2, 80 °C, not nitrogen purged. Lane 6: 4 h reaction without shaking, molar ratio of azide to alkyne primers = 2, 30 °C, nitrogen purged. Lane 7: 4 h reaction shaking at 40 r/min, molar ratio of azide to alkyne primers = 2, 30 °C, nitrogen purged. (D) Purified DNA handles H, L, and S. (E) Final ligation of the DNA handles. (F) AFM imaging of the final DNA handles.

arabinose, but without providing the unnatural amino acid AzF, the protein was not expressed. This indicates that the BL21(DE3) bacterial expression system co-transformed with two plasmids has a reliable background control. After supplementing 1 mmol/L IPTG, 0.02% arabinose, and 1 mmol/L AzF to the culture, the target protein MLL1 AzF-SET was expressed significantly (Figure S5A, lane 3). According to our previous experience, 5% glycerol should be supplemented to increase the concentration of the unnatural amino acid AzF inside the bacterial cells, but there was no significant expression of the target protein MLL1 AzFSET in BL21(DE3) bacteria (Figure S5A, lane 4). When 5% DMSO was substituted for glycerol, the expression level of MLL1 AzF-SET in BL21(DE3) bacteria was slightly lower compared to the condition without DMSO reagent (Figure S5A, lane 5). Under the condition of supplementing 5% glycerol and 5% DMSO, MLL1 AzF-SET showed weak expression (Figure S5A, lane 6).

In short, glycerol or DMSO is not necessary to increase the concentration of the unnatural amino acid AzF inside the bacterial cells which has been argued previously.[13a] BL21(DE3) bacteria can efficiently incorporate AzF without the supplement. The arabinose dose required for regulation by the plasmid pEVOLCNF-RS is relatively low compared to the arabinose induction dose used previous in literature.[13a] A dose of 0.02% is sufficient to induce the expression of the tRNA and aaRS required for the genetic code expansion. In addition, 1 mmol/L IPTG is higher than the previously used dose of 0.2 mmol/L.[13a] Based on the above results, we found the optimized expression conditions as follows: 2xYT medium, culture temperature of 37 °C, induction temperature of 25 °C, IPTG of 1 mmol/L, arabinose of 0.02%, supplemented with 10 μmol/L $ZnCl_2$, and no need for the addition of glycerol or DMSO. We subsequently expressed and purified the MLL1 AzFSET protein in BL21(DE3) bacteria (Figure S5B).

We chose the strain-promoted azide-alkyne cycloaddition (SPAAC) reaction, which does not require copper, for protein-DNA conjugation.[21] When proteins are coupled to nucleic acids using SPAAC click chemistry, we used DNA primers modified with dibenzocyclooctyne (DBCO) (Figure 3A). The MLL1 SET protein carrying AzF was prepared as above. Through SPAAC reaction with a

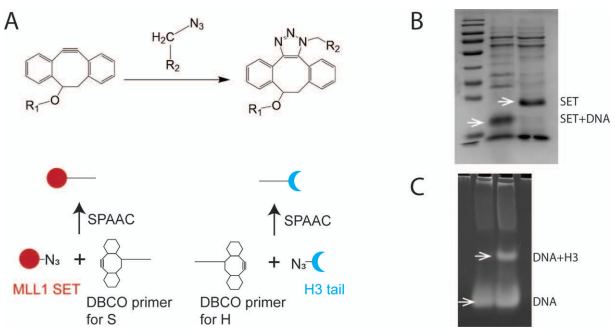

Figure 3 Protein-DNA bioconjugation. (A) Schematic representation of protein-DNA bioconjugation using SPAAC. (B) Bioconjugation of SET and DNA. (C) Bioconjugation of H3 tail and DNA.

DBCO-modified S primer, the protein-DNA conjugate migrated noticeably lower than the protein band in SDS-PAGE gels (Figure 3B). Using the same click chemistry strategy, the H3 tail peptide was conjugated with a DBCO primer, and after non-denaturing PAGE electrophoresis and nucleic acid staining, a noticeable upward shifted band could also be observed (Figure 3C). Based on the guidelines for DNA and protein elution and recovery methods described in the literature,[22] we ran the DNA-protein conjugates on a non-denaturing PAGE gel, excised the target bands, and eluted them by electrophoresis. The products were then subjected to dialysis or concentration using an ultrafiltration or PEG20000 dialysis tube, and the protein-DNA conjugates were collected.

Assembly of the DNA force circuit for PPI

The DNA force circuit for probing MLL1 SET-H3 PPIs in single-molecule assays was assembled through DNA base pairing (Figure 4A). To evaluate the assembly efficiency and the occurrence of high molecular weight byproducts, we performed AFM morphological analysis. To suppress the occurrence of high molecular weight byproducts, we explored the mixing ratios and concentrations of DNA templates, splint oligos, and protein-DNA bioconjugates. The AFM imaging in liquid demonstrated excellent dispersity of the constructed PPI structures, with minimal occurrence of high molecular weight byproducts, and revealed successful overall assembly of the PPI structures, with the target proteins assembled at the expected positions (Figure 4B).

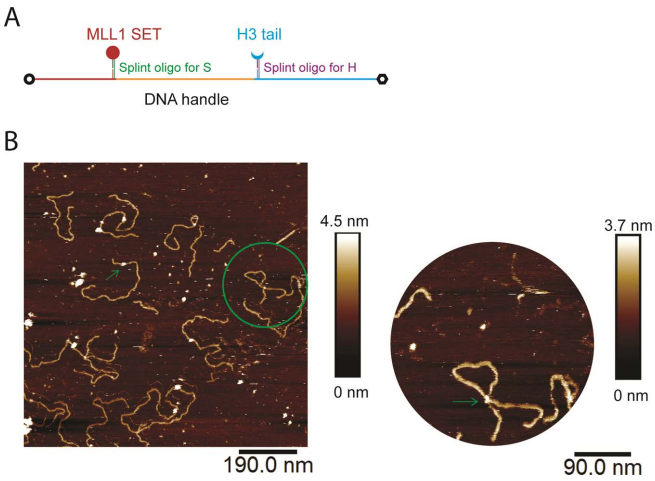

Figure 4 Assembly and characterization of the DNA force circuit. (A) Schematic representation of the assembly of the DNA force circuit. (B) AFM images of the DNA force circuit. The right panel is a zoomed-in view of the circled region in the left panel. Arrows indicate the bioconjugated protein on DNA (left) and the α conformation formed by the DNA force circuit through protein-protein interactions (right).

The MLL1 SET protein consists of 185 amino acids and has a molecular weight of 21.47 kDa. The folded SET protein adopts a spherical shape with a diameter of a few nanometers. The DNA double helix has a diameter of 2 nm. These basic data of the molecules provided essential references for our AFM morphological analysis. We observed that the DNA strands exhibited a height of approximately 1.5 nm and appeared copper-colored, while the protein regions appeared white and exhibited a greater height compared to DNA. The SET protein, prepared using the expanded genetic code technology, was conjugated to the nucleic acid through orthogonally clickable chemistry. The alkyne-modified position on the nucleic acid was located at approximately 1/5 position on one end of the DNA handle. Based on the protein size and the location of nucleic acid conjugation, we concluded that the MLL1 SET protein successfully assembled onto the DNA templates. The assembly position of the H3 peptide on the DNA handle is approximately located at 3/5 position. Therefore, by interacting with the H3 peptide, the MLL1 SET protein causes a conformational change of the DNA handle, resembling an alpha letter (Figure 4B). Following the overall assembly, the PPI structures were phosphorylated using T4 PNK kinase and ligated using T4 DNA ligase before being used in single-molecule manipulation experiments.

Single-molecule signals of PPI by the DNA force circuit

The interaction between MLL1 SET and histone H3 tail within the DNA force circuit was probed using single-molecule magnetic tweezers (Figure 5A). The glass substrate of the sample chamber was coated with anti-digoxigenin antibodies, which served as anchors for the digoxigenin end of the DNA force circuit. The biotin end of the circuit was immobilized onto magnetic beads conjugated with streptavidin. Consequently, one end of the circuit was fixed on the glass substrate, while the other was attached to the surface of the magnetic beads. This allowed us to apply mechanical loads to the DNA force circuit.

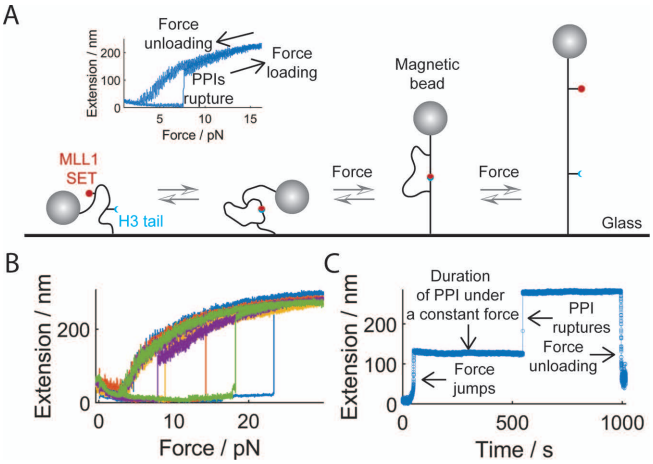

Figure 5 Single-molecule manipulations of the DNA force circuit for detecting MLL1 SET-H3 tail PPIs. (A) Schematic representation of the experimental setup using single-molecule magnetic tweezers and the DNA force circuit. The inset shows a representative force-extension trace. (B) Five force-extension traces reveal rupture events of PPIs in force ramp assays. (C) Representative extension trace demonstrating the duration of a PPI under a constant force in force jump assays.

To investigate the mechanical properties of the MLL1 SET-H3 interaction, we performed force ramp assays on the DNA force circuit in the range of 0—30 pN. We first allowed the MLL1 SET and H3 tail to interact under zero mechanical load and then increased the mechanical load at a rate of 0.5 pN/s. Once the mechanical load reached 30 pN, we unloaded the force back to 0 pN at a rate of −0.5 pN/s. After a few minutes, we repeated the single-molecule force ramp procedure. We observed that mechanical loads could disrupt the PPI between MLL1 SET and histone H3 tail (Figure 5B). The position of the magnetic beads was continuously monitored by the magnetic tweezers to measure the length of the DNA force circuit. The length of the DNA force circuit increased as the mechanical load intensified in accordance with theoretical predictions.[23] The DNA handle L in the parallel circuit was longer than the PPI path, indicating that the PPI path bore the primary mechanical load. When the mechanical load exceeded the strength of the MLL1 SET-H3 interaction, the PPI ruptured, resulting in a sudden leap in the position of the magnetic beads or a sudden extension of the DNA force circuit in the force extension curve. At the same time, DNA handle L experienced a force from zero to the current mechanical load upon PPI ruptured.

Single-molecule force spectroscopy experiments allowed us to investigate the PPIs between MLL1 SET and histone H3 tail over a

wide range of mechanical forces. Moreover, by rapidly changing the mechanical load, we could examine the local non-equilibrium kinetics of the PPIs in force jump assays (Figure 5C). At zero or extremely low mechanical loads, we allowed a certain time for the MLL1 SET protein and histone H3 tail to undergo PPIs. Then, we abruptly increased the mechanical load to a high level. At this moment, we started timing the duration for which the PPI between MLL1 SET and histone H3 tail endured the mechanical load until the PPI ruptured, thereby obtaining the dissociation time of the PPI at a constant force.

Discussion

Epigenetic modifications, including methylation, acetylation, phosphorylation, among others, have been shown to influence the PPIs of transcription factors, thus regulating gene expression.[24] The mixed-lineage leukemia protein MLL1 plays an essential role in the top-level control of transcription and is the first member of the KMT2 family identified.[25] The MLL1 protein contains several drug-targeting domains of great interest, including CXXC, PHDs, Bromo domain, and SET.[26] Of particular importance is the SET domain, which houses the catalytic center responsible for MLL1-mediated methylation of histone proteins, rendering it a significant target for epigenetic drug discovery endeavors.[15a,27]

The formation of a complex involving the SET domain of MLL1, the cofactor, and a histone H3 peptide is well-established. Traditional approaches based on biochemical and molecular biology techniques have yielded ensemble-averaged parameters characterizing this complex. To further examine the interaction dynamics, we implemented a novel experimental approach using magnetic tweezers and AFM to measure the forces and durations of the PPIs of MLL1 SET with its H3 substrate at the single-molecule level. Previously, we have demonstrated a parallel DNA circuit to explore the organization of telomeric DNA at the single-molecule level, discovering that single-stranded overhangs at telomeric ends can form triplex structures through unfolding events with upstream double-stranded DNA.[28] Additionally, this single-molecule DNA force circuit can also be employed to study nucleic acid drugs targeting the HIV genome, evaluating the mechanical stability and specificity of drug-nucleic acid interactions. Moreover, we used the DNA force circuit to investigate the PPIs between the PHD3-Bromo domain of MLL1 and its histone substrate.[13a]

To further improve the DNA force circuit, we optimized its construction using click chemistry and genetic code expansion techniques. Click chemistry offers high biocompatibility and specificity for biological conjugation, making it an invaluable tool in our research. Genetic code expansion technology, on the other hand, allows for the introduction of unnatural amino acids into proteins, providing enhanced biocompatibility and biological orthogonality while enabling site-specific and stoichiometric control over conjugation reactions.[29] Through atomic force microscopy morphology analysis, we were able to evaluate the critical steps in the development of methods during the preparation and assembly of PPI structures. After optimizing the preparation and assembly procedure of single-molecule PPI structures in this study, the efficiency of bioconjugate reactions has been improved, as well as the efficiency of protein engineering using expanded genetic codes to introduce unnatural amino acids.

Utilizing DNA as a scaffold for probing PPIs offers two main advantages. Firstly, DNA modules with clickable nucleotides provide flexibility by enabling a wide range of manipulation geometries on PPIs. This is accomplished through the incorporation of unnatural amino acids into the two proteins of interest, which allows for the achievement of numerous mechanical manipulation geometries via bioconjugation between protein and DNA using click chemistry. Secondly, DNA modules are scalable in size, enabling convenient adjustment of the DNA length to accommodate variable designs of the PPI construct. We have designed an additional circuit preparation flowchart of a PPI construct using longer DNAs and included its AFM characterization of the DNA scaffold (Figure S6), demonstrating the versatility and adaptability of the DNA scaffold.

Conclusions

The single-molecule mechanical PPI method developed in this study not only expands the toolbox for studying PPIs but also offers a novel experimental approach for elucidating the enzymatic mechanisms of epigenetic drug targets. We anticipate that our single-molecule mechanical method is not limited to the field of PPIs but also holds potential applicability in the broader field of drug discovery.

Experimental

Other than expressly noted, we have purchased all chemicals from Sigma-Aldrich and enzymes from New England Biolabs.

MD simulation

The all-atom dynamics simulation of the pulling process was performed using the GROMACS-2022.4 software package.[15b] We obtained the initial structure of the simulation system, force field parameters (CHARMM36m force field[15c]), using the CHARMM-GUI web server.[15d] The initial coordinates of MLL1 and the substrate were obtained from the PDB entry 2W5Z. In the initial structure of the simulation system, water was modeled using the TIP3P model. Protonation of MLL1 and its substrate (pH 7.4) was performed, and 100 mmol/L NaCl was added to neutralize the system's charge. The entire system consisted of approximately 160 000 atoms. To calculate electrostatic interactions, the particle mesh Ewald method was employed, while electrostatic and van der Waals interactions were truncated at a length of 12 Å. The LINCS algorithm was used to constrain bonds involving hydrogen atoms.

For simulating the pulling of the substrate in different directions, first, the system energy was minimized using the steepest descent algorithm until the force reached less than 1000 (kJ/mol)/nm. Next, a NVT equilibration was carried out for 125 ps using the Velocity-rescale thermostat at 294.15 K with a time step of 1 fs. To facilitate the pulling process, harmonic position restraints were applied to the α-C atoms of the H3 peptide with a spring constant of 500 (kJ/mol)/nm^2. Specifically, the α-C atoms of 2-THR, 4-GLN, 5-THR, and 8-TYR were selected as the force application points, with a constant force of 200 (kJ/mol)/nm applied. Upon determining the pulling parameters, the system underwent a pulling simulation in the NPT ensemble with a time step of 2 fs using the Velocity-rescale thermostat and Berendsen isotropic barostat.

Expression and purification of MLL1 AzF-SET

From professor Ming Lei (Shanghai Jiao Tong University), we obtained the sequence of MLL1 SET (Table S1).[25d] To introduce site-specific mutagenesis in the MLL1 SET domain, we utilized a Hieff Mut™ kit (Cat#: 11003ES10, Yeasen Biotech, China) to mutate the codon of the targeted amino acid to an amber stop codon (TAG).

For the expression and purification of the MLL1 AzF-SET domain, we initially transformed and induced cells, followed by cell lysis using an ultrasonic cell crusher (Scientz-IID, SCIENTZ, China) in a PBS buffer (pH 7.4). The cell lysate was then subjected to centrifugation, and the resulting supernatant was passed through a resin (Cat#: 17531806, Ni Sepharose 6 Fast Flow, GE Healthcare, USA) capable of binding 6xHis tags. Subsequently, extensive washing with 20 mmol/L imidazole was performed to remove nonspecifically bound proteins.

To elute the MLL1 AzF-SET protein, an elution buffer contain-

ing a linear gradient of imidazole (50—300 mmol/L) was used. The elution buffer was then exchanged to PBS using Amicon Ultra centrifugal filter units (Cat#: UFC903024, Millipore, USA). The protein was further purified by binding to a resin (Cat#: 17075601, GE) through GST tags, which were later cleaved using HRV 3C protease (Cat#: 88946, Thermo Fisher, USA).

To confirm the successful expression and purification of the MLL1 AzF-SET protein, SDS-Polyacrylamide gel electrophoresis (PAGE) and Western blot analysis using an anti-6xHis tag antibody (Cat#: ab9108, Abcam, USA) were performed. The final purified product, MLL1 AzF-SET (300—500 μmol/L), was stored at −80 °C.

Engineering the DNA force circuit

The DNA force circuit was engineered using a CuAAC approach to create branched conjugates of DNA oligos. Commercially available azide and alkyne modified DNA oligos from Sangon Biotech were used (Table S2). The CuAAC reaction was performed by mixing an alkyne-DNA oligo and an azide-DNA oligo in a 50 μL solution containing 10 mmol/L tris[(1-benzyl-1*H*-1,2,3-triazol-4-yl)methyl]amine (TBTA), 20 mmol/L sodium ascorbate, and 2.5 mmol/L $CuSO_4$. The reaction was quenched by adding 1 μL of 500 mmol/L EDTA. The resulting branched conjugates of DNA oligos were separated and purified using denaturing urea PAGE with a 0.5× TBE buffer. After ethanol precipitation, the branched primers were recovered and stored at −20 °C.

To generate double-stranded DNA (dsDNA) handles for the PPI construct, branched primers were used in a PCR reaction with λ-DNA as templates. Biotin or digoxigenin modified paired primers were included in the PCR to produce biotin or digoxigenin handles. The DNA handles and the flexible linker were ligated using T4 DNA ligase at the restriction sites of BbvcI and BssSa I.

Protein-DNA conjugation was achieved through copper-free click chemistry using SPAAC. The click reaction was initiated by mixing the DBCO oligo (General Biosystems, Inc.) and azide-modified MLL1 SET in PBS (pH 7.4). The conjugate was purified by electroelution using a D-tube Dialyzer (MWCO = 3.5 kDa, Millipore) followed by buffer exchange using an Amicon filter (Millipore) before storing in PBS at −20 °C. A similar click reaction was performed to prepare the conjugate of H3-DNA using DBCO-modified DNA oligo (General Biosystems, Inc.) and azide-modified H3K4me3 tail (Shanghai Top-Peptide Biotechnology, China) (Table S1).

The assembly of the final PPI construct involved annealing the DNA handles and the protein-DNA conjugate by heating to 65 °C and gradual cooling to 4 °C. The nick at the branched DNA was ligated using T4 DNA ligase. The PPI construct was isolated through agarose gel electrophoresis, followed by gel cutting, electroelution, and Amicon filter-based buffer exchange. The final PPI construct of the DNA force circuit was stored in a buffer of 10 mmol/L Tris (pH 8) with 100 mmol/L NaCl at −20 °C.

AFM imaging

The AFM instrument used in this study was the Multimode 8 (MM8) manufactured by Bruker. Sample preparation for AFM imaging followed a procedure published in literature.[30] Prior to AMF imaging, 100 μL of 100 mmol/L $NiCl_2$, 20 mL of deposition buffer (containing 10 mmol/L HEPES adjusted with KOH, 10 mmol/L $MgCl_2$, and 25 mmol/L KCl), and 5 mL of imaging buffer (containing 10 mmol/L HEPES adjusted with KOH, 10 mmol/L $NiCl_2$, and 25 mmol/L KCl) were freshly prepared. To prepare the mica surface, adhesive tape was used to peel it, ensuring its freshness. Then, 20 μL of 100 mmol/L $NiCl_2$ was immediately pipetted onto the mica surface, followed by a 1-minute incubation. The mica surface was then rinsed with 50 mL of autoclaved MilliQ water, and excess water was carefully removed using tissue paper. Subsequently, 20 μL of 0.5 ng/μL DNA was pipetted onto the mica surface. The DNA was initially rinsed with 1 mL of deposition buffer, followed by further rinsing with 8 mL of deposition buffer while tilting the mica from a flat to an inclined position. Finally, the mica surface was rinsed with 2 mL of imaging buffer, leaving a volume of 120 μL droplets on the surface for subsequent AFM imaging.

For high XY resolution, a 2 nm tip, such as the ScanAsyst Fluid+ probe or the SNL-10 probe manufactured by Bruker, was recommended. The Amplitude setpoint was optimized to ensure that the trace and retrace curves closely matched each other. Additionally, adjustments were made to the Integral gain and Proportional gain parameters to achieve a close alignment of the trace and retrace curves without any oscillations. Gradually increasing the scanning range from 10 nm was done to determine the appropriate scan size, accompanied by a decrease in scan rate as the scanning range increased. Image analysis was carried out using NanoScope software and FiberApp.[31]

Single-molecule manipulations using magnetic tweezers

We employed custom-made magnetic tweezers,[9b,11a,28] consisting of a microscopy system, motor-controlling magnets, and a flow cell connected to a pump. Single-molecule experiments were conducted using a microsphere-DNA-coverslip setup within a microfluidic chamber. Typically, we mixed 0.1 ng of PPI construct with 10 μL of streptavidin-coated microspheres (Cat#: 65305, M270, Invitrogen, USA) in 40 μL of PBS buffer (pH 7.4) or Tris buffer (pH 8.0, 10 mmol/L Tris, 100 mmol/L NaCl). The coverslip was coated with a 0.1% g/mL nitrocellulose matrix, and subsequently passivated with BSA (5 mg/mL) overnight. The PPI construct was immobilized between the coverslip surface and microspheres. Single-molecule manipulation assays were performed at a sampling rate of 200 Hz, using a PBS buffer (pH 7.4) or Tris buffer (pH 8.0) supplemented with 10 μmol/L $ZnCl_2$ and 0.00315% Tween 20. Data analysis was conducted using Matlab 2022a (MathWorks, USA), unless otherwise stated explicitly.

Supporting Information

The supporting information for this article is available on the WWW under https://doi.org/10.1002/cjoc.202300723.

Acknowledgement

We thank Professor Ming Lei (Shanghai Jiao Tong University) for the plasmid containing the MLL1 SET sequence. We would like to express our gratitude to Professor Weimin Xuan (Tianjin University) for providing us with the plasmid pEVOLCNF-RS. This work was supported by the National Natural Science Foundation of China [Grant 32071227 to Z.Y.; Grant 12275137 to Y.L.], Tianjin Municipal Natural Science Foundation of China (22JCYBJC01070 to Z.Y.), and State Key Laboratory of Precision Measuring Technology and Instruments (Tianjin University) [Grant pilab2210 to Z.Y.].

References

[1] (a) Scott, D. E.; Bayly, A. R.; Abell, C.; Skidmore, J. Small molecules, big targets: drug discovery faces the protein-protein interaction challenge. *Nat. Rev. Drug Discov.* **2016**, *15*, 533–550; (b) Corbi-Verge, C.; Garton, M.; Nim, S.; Kim, P. M. Strategies to Develop Inhibitors of Motif-Mediated Protein-Protein Interactions as Drug Leads. *Annu. Rev. Pharmacol. Toxicol.* **2017**, *57*, 39–60; (c) Sheng, C.; Dong, G.; Miao, Z.; Zhang, W.; Wang, W. State-of-the-art strategies for targeting protein-protein interactions by small-molecule inhibitors. *Chem. Soc. Rev.* **2015**, *44*, 8238–8259.

[2] (a) Bosc, N.; Muller, C.; Hoffer, L.; Lagorce, D.; Bourg, S.; Derviaux, C.; Gourdel, M. E.; Rain, J. C.; Miller, T. W.; Villoutreix, B. O.; Miteva, M. A.; Bonnet, P.; Morelli, X.; Sperandio, O.; Roche, P. Fr-PPIChem: An Academic Compound Library Dedicated to Protein-Protein Interactions. *ACS Chem. Biol.* **2020**, *15*, 1566–1574; (b) Ivanov, A. A.;

Revennaugh, B.; Rusnak, L.; Gonzalez-Pecchi, V.; Mo, X.; Johns, M. A.; Du, Y.; Cooper, L. A. D.; Moreno, C. S.; Khuri, F. R.; Fu, H. The OncoPPi Portal: an integrative resource to explore and prioritize protein-protein interactions for cancer target discovery. *Bioinformatics* **2018**, *34*, 1183–1191.

[3] (a) Wolter, M.; Valenti, D.; Cossar, P. J.; Levy, L. M.; Hristeva, S.; Genski, T.; Hoffmann, T.; Brunsveld, L.; Tzalis, D.; Ottmann, C. Fragment-Based Stabilizers of Protein-Protein Interactions through Imine-Based Tethering. *Angew. Chem. Int. Ed.* **2020**, *59*, 21520–21524; (b) Kitel, R.; Rodríguez, I.; Del Corte, X.; Atmaj, J.; Żarnik, M.; Surmiak, E.; Muszak, D.; Magiera-Mularz, K.; Popowicz, G. M.; Holak, T. A.; Musielak, B. Exploring the Surface of the Ectodomain of the PD-L1 Immune Checkpoint with Small-Molecule Fragments. *ACS Chem. Biol.* **2022**, *17*, 2655–2663; (c) Renzi, F.; Seamann, A.; Ganguly, K.; Pandey, K.; Byrareddy, S. N.; Batra, S.; Kumar, S.; Ghersi, D. Engineering an ACE2-Derived Fragment as a Decoy for Novel SARS-CoV-2 Virus. *ACS Pharmacol. Transl. Sci.* **2023**, *6*, 857–867; (d) Tang, S.; Kim, P. S. A high-affinity human PD-1/PD-L2 complex informs avenues for small-molecule immune checkpoint drug discovery. *Proc. Natl. Acad. Sci. U. S. A.* **2019**, *116*, 24500–24506; (e) Rego, N. B.; Xi, E.; Patel, A. J. Identifying hydrophobic protein patches to inform protein interaction interfaces. *Proc. Natl. Acad. Sci. U. S. A.* **2021**, *118*, e2018234118.

[4] (a) Gerry, C. J.; Schreiber, S. L. Unifying principles of bifunctional, proximity-inducing small molecules. *Nat. Chem. Biol.* **2020**, *16*, 369–378; (b) Jones, S.; Thornton, J. M. Principles of protein-protein interactions. *Proc. Natl. Acad. Sci. U. S. A.* **1996**, *93*, 13–20; (c) Zhong, M.; Lynch, A.; Muellers, S. N.; Jehle, S.; Luo, L.; Hall, D. R.; Iwase, R.; Carolan, J. P.; Egbert, M.; Wakefield, A.; Streu, K.; Harvey, C. M.; Ortet, P. C.; Kozakov, D.; Vajda, S.; Allen, K. N.; Whitty, A. Interaction Energetics and Druggability of the Protein-Protein Interaction between Kelch-like ECH-Associated Protein 1 (KEAP1) and Nuclear Factor Erythroid 2 Like 2 (Nrf2). *Biochemistry* **2020**, *59*, 563–581; (d) Stevers, L. M.; de Vink, P. J.; Ottmann, C.; Huskens, J.; Brunsveld, L. A Thermodynamic Model for Multivalency in 14–3-3 Protein-Protein Interactions. *J. Am. Chem. Soc.* **2018**, *140*, 14498–14510; (e) Plattner, N.; Doerr, S.; De Fabritiis, G.; Noé, F. Complete protein-protein association kinetics in atomic detail revealed by molecular dynamics simulations and Markov modelling. *Nat. Chem.* **2017**, *9*, 1005–1011.

[5] (a) Copeland, R. A. The drug-target residence time model: a 10-year retrospective. *Nat. Rev. Drug Discov.* **2016**, *15*, 87–95; (b) Yang, T.; Cuesta, A.; Wan, X.; Craven, G. B.; Hirakawa, B.; Khamphavong, P.; May, J. R.; Kath, J. C.; Lapek, J. D., Jr.; Niessen, S.; Burlingame, A. L.; Carelli, J. D.; Taunton, J. Reversible lysine-targeted probes reveal residence time-based kinase selectivity. *Nat. Chem. Biol.* **2022**, *18*, 934–941; (c) Tiwary, P.; Mondal, J.; Berne, B. J. How and when does an anticancer drug leave its binding site? *Sci. Adv.* **2017**, *3*, e1700014; (d) Sabatier, P.; Beusch, C. M.; Meng, Z.; Zubarev, R. A. System-Wide Profiling by Proteome Integral Solubility Alteration Assay of Drug Residence Times for Target Characterization. *Anal. Chem.* **2022**, *94*, 15772–15780; (e) Renaud, J. P.; Chung, C. W.; Danielson, U. H.; Egner, U.; Hennig, M.; Hubbard, R. E.; Nar, H. Biophysics in drug discovery: impact, challenges and opportunities. *Nat. Rev. Drug Discov.* **2016**, *15*, 679–698; (f) Wang, J.; Li, S.; Li, H. Drug Design of "Undruggable" Targets. *Chin. J. Chem.* **2019**, *37*, 501–512.

[6] (a) Shank, E. A.; Cecconi, C.; Dill, J. W.; Marqusee, S.; Bustamante, C. The folding cooperativity of a protein is controlled by its chain topology. *Nature* **2010**, *465*, 637–640; (b) Jagannathan, B.; Elms, P. J.; Bustamante, C.; Marqusee, S. Direct observation of a force-induced switch in the anisotropic mechanical unfolding pathway of a protein. *Proc. Natl. Acad. Sci. U. S. A.* **2012**, *109*, 17820–17825; (c) Li, Y. D.; Lamour, G.; Gsponer, J.; Zheng, P.; Li, H. The molecular mechanism underlying mechanical anisotropy of the protein GB1. *Biophys. J.* **2012**, *103*, 2361–2368; (d) Schweitzer, Y.; Kozlov, M. M. Membrane-mediated interaction between strongly anisotropic protein scaffolds. *PLoS Comput. Biol.* **2015**, *11*, e1004054.

[7] (a) Strick, T. R.; Yan, J. A measure of force. *Curr. Opin. Chem. Biol.* **2019**, *53*, A4–A6; (b) Wang, Y.; Yan, J.; Goult, B. T. Force-Dependent Binding Constants. *Biochemistry* **2019**, *58*, 4696–4709; (c) Lipfert, J.; van Oene, M. M.; Lee, M.; Pedaci, F.; Dekker, N. H. Torque spectroscopy for the study of rotary motion in biological systems. *Chem. Rev.* **2015**, *115*, 1449–1474.

[8] (a) Strick, T. R.; Croquette, V.; Bensimon, D. Single-molecule analysis of DNA uncoiling by a type II topoisomerase. *Nature* **2000**, *404*, 901–904; (b) Douglass, A. D.; Vale, R. D. Single-molecule microscopy reveals plasma membrane microdomains created by protein-protein networks that exclude or trap signaling molecules in T cells. *Cell* **2005**, *121*, 937–950; (c) Koster, D. A.; Croquette, V.; Dekker, C.; Shuman, S.; Dekker, N. H. Friction and torque govern the relaxation of DNA supercoils by eukaryotic topoisomerase IB. *Nature* **2005**, *434*, 671–674; (d) Vera, A. M.; Carrion-Vazquez, M. Direct Identification of Protein-Protein Interactions by Single-Molecule Force Spectroscopy. *Angew. Chem. Int. Ed.* **2016**, *55*, 13970–13973.

[9] (a) Yang, L.; Zhang, Z.; Zhao, C.; Huo, Y.; Zhang, E.; He, S.; Jia, C.; Guo, X. Monitoring Molecular Dynamics with Single-Molecule Electronic Devices and Fluorescence Techniques. *Chin. J. Chem.* **2023**, *41*, 2889–2907; (b) Wang, Z.; Cao, Z.; Ma, K.; Lu, M.; Wang, M.; Gao, H.; Gong, D.; Liang, L.; Yu, Z. Reading Time and DNA Sequence Preference of TET3 CXXC Domain Revealed by Single-Molecule Profiling. *Chin. J. Chem.* **2023**, *41*, 1177–1184.

[10] (a) Janissen, R.; Berghuis, B. A.; Dulin, D.; Wink, M.; van Laar, T.; Dekker, N. H. Invincible DNA tethers: covalent DNA anchoring for enhanced temporal and force stability in magnetic tweezers experiments. *Nucleic Acids Res.* **2014**, *42*, e137; (b) Li, X.; Wang, M.; Zheng, W.; Huang, W.; Wang, Z.; Jin, K.; Liu, L.; Yu, Z. Dynamics of TRF1 organizing a single human telomere. *Nucleic Acids Res.* **2021**, *49*, 760–775.

[11] (a) Liang, L.; Ma, K.; Wang, Z.; Janissen, R.; Yu, Z. Dynamics and inhibition of MLL1 CXXC domain on DNA revealed by single-molecule quantification. *Biophys. J.* **2021**, *120*, 3283–3291; (b) Liang, L.; Wang, Z.; Qu, L.; Huang, W.; Guo, S.; Guan, X.; Zhang, W.; Sun, F.; Yuan, H.; Zou, H.; Liu, H.; Yu, Z. Single-molecule multiplexed profiling of protein-DNA complexes using magnetic tweezers. *J. Biol. Chem.* **2021**, *296*, 100327.

[12] (a) Wang, Y.; Barnett, S. F. H.; Le, S.; Guo, Z.; Zhong, X.; Kanchanawong, P.; Yan, J. Label-free Single-Molecule Quantification of Rapamycin-induced FKBP-FRB Dimerization for Direct Control of Cellular Mechanotransduction. *Nano Lett.* **2019**, *19*, 7514–7525; (b) Bauer, M. S.; Gruber, S.; Hausch, A.; Gomes, P.; Milles, L. F.; Nicolaus, T.; Schendel, L. C.; Navajas, P. L.; Procko, E.; Lietha, D.; Melo, M. C. R.; Bernardi, R. C.; Gaub, H. E.; Lipfert, J. A tethered ligand assay to probe SARS-CoV-2:ACE2 interactions. *Proc. Natl. Acad. Sci. U. S. A.* **2022**, *119*, e2114397119.

[13] (a) Ma, X.; Zhu, M.; Liu, J.; Li, X.; Qu, L.; Liang, L.; Huang, W.; Wang, J.; Li, N.; Chen, J. H.; Zhang, W.; Yu, Z. Interactions between PHD3-Bromo of MLL1 and H3K4me3 Revealed by Single-Molecule Magnetic Tweezers in a Parallel DNA Circuit. *Bioconjug. Chem.* **2019**, *30*, 2998–3006; (b) Kostrz, D.; Wayment-Steele, H. K.; Wang, J. L.; Follenfant, M.; Pande, V. S.; Strick, T. R.; Gosse, C. A modular DNA scaffold to study protein–protein interactions at single-molecule resolution. *Nat. Nanotechnol.* **2019**, *14*, 988–993.

[14] (a) Zhang, J.; Dong, J. Modular Click Chemistry Library: Searching for Better Functions. *Chin. J. Chem.* **2021**, *39*, 1025–1027; (b) Xu, L.; Dong, J. Click Chemistry: Evolving on the Fringe. *Chin. J. Chem.* **2020**, *38*, 414–419; (c) Sun, F.; Zhang, W.-B. Genetically Encoded Click Chemistry. *Chin. J. Chem.* **2020**, *38*, 894–896.

[15] (a) Southall, S. M.; Wong, P. S.; Odho, Z.; Roe, S. M.; Wilson, J. R. Structural basis for the requirement of additional factors for MLL1 SET domain activity and recognition of epigenetic marks. *Mol. Cell* **2009**, *33*, 181–191; (b) Abraham, M. J.; Murtola, T.; Schulz, R.; Páll, S.; Smith, J. C.; Hess, B.; Lindahl, E. GROMACS: High performance molecular simulations through multi-level parallelism from laptops to supercomputers. *SoftwareX* **2015**, *1–2*, 19–25; (c) Huang, J.; Rauscher, S.; Nawrocki, G.; Ran, T.; Feig, M.; de Groot, B. L.; Grubmüller, H.; MacKerell, A. D. CHARMM36m: an improved force field for folded and intrinsically disordered proteins. *Nat. Methods*

2017, *14*, 71–73; (d) Allouche, A. R. Gabedit—A graphical user interface for computational chemistry softwares. *J. Comput. Chem.* **2011**, *32*, 174–182.
[16] (a) Kolb, H. C.; Finn, M. G.; Sharpless, K. B. Click Chemistry: Diverse Chemical Function from a Few Good Reactions. *Angew. Chem. Int. Ed.* **2001**, *40*, 2004–2021; (b) Agrahari, A. K.; Bose, P.; Jaiswal, M. K.; Rajkhowa, S.; Singh, A. S.; Hotha, S.; Mishra, N.; Tiwari, V. K. Cu(I)-Catalyzed Click Chemistry in Glycoscience and Their Diverse Applications. *Chem. Rev.* **2021**, *121*, 7638–7956.
[17] (a) Liu, C. C.; Schultz, P. G. Adding new chemistries to the genetic code. *Annu. Rev. Biochem.* **2010**, *79*, 413–444; (b) Wang, L.; Xie, J.; Schultz, P. G. Expanding the genetic code. *Annu. Rev. Biophys. Biomol. Struct.* **2006**, *35*, 225–249; (c) Wang, L.; Brock, A.; Herberich, B.; Schultz, P. G. Expanding the genetic code of *Escherichia coli*. *Science* **2001**, *292*, 498–500.
[18] Chatterjee, A.; Sun, S. B.; Furman, J. L.; Xiao, H.; Schultz, P. G. A versatile platform for single- and multiple-unnatural amino acid mutagenesis in *Escherichia coli*. *Biochemistry* **2013**, *52*, 1828–1837.
[19] Chin, J. W.; Santoro, S. W.; Martin, A. B.; King, D. S.; Wang, L.; Schultz, P. G. Addition of p-Azido-l-phenylalanine to the Genetic Code of Escherichia coli. *J. Am. Chem. Soc.* **2002**, *124*, 9026–9027.
[20] Young, D. D.; Young, T. S.; Jahnz, M.; Ahmad, I.; Spraggon, G.; Schultz, P. G. An Evolved Aminoacyl-tRNA Synthetase with Atypical Polysubstrate Specificity. *Biochemistry* **2011**, *50*, 1894–1900.
[21] (a) Reddington, S. C.; Tippmann, E. M.; Dafydd Jones, D. Residue choice defines efficiency and influence of bioorthogonal protein modification via genetically encoded strain promoted Click chemistry. *Chem. Commun.* **2012**, *48*, 8419–8421; (b) Marth, G.; Hartley, A. M.; Reddington, S. C.; Sargisson, L. L.; Parcollet, M.; Dunn, K. E.; Jones, D. D.; Stulz, E. Precision Templated Bottom-Up Multiprotein Nanoassembly through Defined Click Chemistry Linkage to DNA. *ACS Nano* **2017**, *11*, 5003–5010; (c) Jewett, J. C.; Bertozzi, C. R. Cu-free click cycloaddition reactions in chemical biology. *Chem. Soc. Rev.* **2010**, *39*, 1272–1279.
[22] (a) Dunn, M. J. Electroelution of proteins from polyacrylamide gels. *Methods Mol. Biol.* **2004**, *244*, 339–343; (b) Sambrook, J.; Russell, D. W. Recovery of DNA from agarose and polyacrylamide gels: electroelution into dialysis bags. *CSH Protoc.* **2006**, *2006*, pdb.prot4023.
[23] (a) Smith, S. B.; Finzi, L.; Bustamante, C. Direct mechanical measurements of the elasticity of single DNA molecules by using magnetic beads. *Science* **1992**, *258*, 1122–1126; (b) Strick, T. R.; Allemand, J. F.; Bensimon, D.; Bensimon, A.; Croquette, V. The elasticity of a single supercoiled DNA molecule. *Science* **1996**, *271*, 1835–1837; (c) Gosse, C.; Croquette, V. Magnetic tweezers: micromanipulation and force measurement at the molecular level. *Biophys. J.* **2002**, *82*, 3314–3329.
[24] (a) Szyf, M. Epigenetics, DNA Methylation, and Chromatin Modifying Drugs. *Ann. Rev. Pharmacol. Toxicol.* **2009**, *49*, 243–263; (b) Gershman, A.; Sauria, M. E. G.; Guitart, X.; Vollger, M. R.; Hook, P. W.; Hoyt, S. J.; Jain, M.; Shumate, A.; Razaghi, R.; Koren, S.; Altemose, N.; Caldas, G. V.; Logsdon, G. A.; Rhie, A.; Eichler, E. E.; Schatz, M. C.; O'Neill, R. J.; Phillippy, A. M.; Miga, K. H.; Timp, W. Epigenetic patterns in a complete human genome. *Science* **2022**, *376*, eabj5089; (c) Patel, D. J.; Wang, Z. Readout of epigenetic modifications. *Annu. Rev. Biochem.* **2013**, *82*, 81–118.
[25] (a) Erfurth, F. E.; Popovic, R.; Grembecka, J.; Cierpicki, T.; Theisler, C.; Xia, Z. B.; Stuart, T.; Diaz, M. O.; Bushweller, J. H.; Zeleznik-Le, N. J. MLL protects CpG clusters from methylation within the Hoxa9 gene, maintaining transcript expression. *Proc. Natl. Acad. Sci. U. S. A.* **2008**, *105*, 7517–7522; (b) Milne, T. A.; Kim, J.; Wang, G. G.; Stadler, S. C.; Basrur, V.; Whitcomb, S. J.; Wang, Z.; Ruthenburg, A. J.; Elenitoba-Johnson, K. S.; Roeder, R. G.; Allis, C. D. Multiple interactions recruit MLL1 and MLL1 fusion proteins to the HOXA9 locus in leukemogenesis. *Mol. Cell.* **2010**, *38*, 853–863; (c) Rao, R. C.; Dou, Y. Hijacked in cancer: the KMT2 (MLL) family of methyltransferases. *Nat. Rev. Cancer* **2015**, *15*, 334–346; (d) Li, Y.; Han, J.; Zhang, Y.; Cao, F.; Liu, Z.; Li, S.; Wu, J.; Hu, C.; Wang, Y.; Shuai, J.; Chen, J.; Cao, L.; Li, D.; Shi, P.; Tian, C.; Zhang, J.; Dou, Y.; Li, G.; Chen, Y.; Lei, M. Structural basis for activity regulation of MLL family methyltransferases. *Nature* **2016**, *530*, 447–452.
[26] Dawson, M. A. The cancer epigenome: Concepts, challenges, and therapeutic opportunities. *Science* **2017**, *355*, 1147–1152.
[27] (a) Zhang, Y.; Mittal, A.; Reid, J.; Reich, S.; Gamblin, S. J.; Wilson, J. R. Evolving Catalytic Properties of the MLL Family SET Domain. *Structure* **2015**, *23*, 1921–1933; (b) Wang, Z.; Song, J.; Milne, T. A.; Wang, G. G.; Li, H.; Allis, C. D.; Patel, D. J. Pro isomerization in MLL1 PHD3-bromo cassette connects H3K4me readout to CyP33 and HDAC-mediated repression. *Cell* **2010**, *141*, 1183–1194.
[28] Li, N.; Wang, J.; Ma, K.; Liang, L.; Mi, L.; Huang, W.; Ma, X.; Wang, Z.; Zheng, W.; Xu, L.; Chen, J.-H.; Yu, Z. The dynamics of forming a triplex in an artificial telomere inferred by DNA mechanics. *Nucleic Acids Res.* **2019**, *47*, e86-e86.
[29] (a) Yang, X.; Zhao, L.; Wang, Y.; Ji, Y.; Su, X. C.; Ma, J. A.; Xuan, W. Constructing Photoactivatable Protein with Genetically Encoded Photocaged Glutamic Acid. *Angew. Chem. Int. Ed.* **2023**, *62*, e202308472; (b) Cao, W.; Qin, X.; Wang, Y.; Dai, Z.; Dai, X.; Wang, H.; Xuan, W.; Zhang, Y.; Liu, Y.; Liu, T. A General Supramolecular Approach to Regulate Protein Functions by Cucurbit[7]uril and Unnatural Amino Acid Recognition. *Angew. Chem. Int. Ed.* **2021**, *60*, 11196–11200.
[30] Heenan, P. R.; Perkins, T. T. Imaging DNA Equilibrated onto Mica in Liquid Using Biochemically Relevant Deposition Conditions. *ACS Nano* **2019**, *13*, 4220–4229.
[31] Usov, I.; Mezzenga, R. FiberApp: An Open-Source Software for Tracking and Analyzing Polymers, Filaments, Biomacromolecules, and Fibrous Objects. *Macromolecules* **2015**, *48*, 1269–1280.

Manuscript received: December 5, 2023
Manuscript revised: January 29, 2024
Manuscript accepted: February 2, 2024
Version of record online: XXXX, 2024

The Authors

Left to Right: Kangkang Ma, Luoan Xiong, Zhuofei Wang, Xin Hu, Lihua Qu, Xuetong Zhao, Yao Li, Zhongbo Yu

